Extended Lyα emission from a damped Lyα absorber at $z = 1.93$, and the relation between damped Lyα absorbers and Lyman-break galaxies

J. U. Fynbo,[1,2,3] P. Møller[1,3]* and S. J. Warren[4]

[1]*European Southern Observatory, Karl-Schwarzschild-Straße 2, D-85748 Garching, Germany*
[2]*Institute of Physics and Astronomy, University of Århus, DK-8000 Århus C, Denmark*
[3]*Space Telescope Science Institute, 3700 San Martin Drive, Baltimore, MD 21218, USA*
[4]*Blackett Laboratory, Imperial College of Science Technology and Medicine, Prince Consort Road, London SW7 2BZ*

ABSTRACT

The number of damped Lyα absorbers (DLAs) currently known is about 100, but our knowledge of their sizes and morphologies is still very sparse, as very few have been detected in emission. Here we present narrow-band and broad-band observations of a DLA in the field of the quasar pair Q0151+048A (qA) and Q0151+048B (qB). These two quasars have very similar redshifts, $z_{em} = 1.922$ and 1.937 respectively, and an angular separation of 3.27 arcsec. The spectrum of qA contains a DLA at $z_{abs} = 1.9342$ (close to the emission redshift) which shows an emission line in the trough, detected at 4σ. Our narrow-band image confirms this detection, and we find Lyα emission from an extended area covering 6×3 arcsec^2, corresponding to $25 \times 12 \, h^{-2}$ kpc^2 ($q_0 = 0.5$, $H_0 = 100 \, h \, \text{km s}^{-1}$). The total Lyα luminosity from the DLA is $1.2 \times 10^{43} \, h^{-2}$ erg s^{-1}, which is several times higher than the Lyα luminosity found from other DLAs. The narrow-band image also indicates that qB is not covered by the DLA. This fact, together with the large equivalent width of the emission line from the Lyα cloud, the large luminosity, and the ~ 300 km s^{-1} blueshift relative to the DLA, can plausibly be explained if qB is the source of ionizing photons, lying to the near side of the DLA at a distance from the DLA of $< 20 \, h^{-1}$ kpc. In this case the size of the emission-line region corresponds to the area over which the cloud is optically thick, i.e., is indicative of the size of a Lyman-limit system. We also consider the relation between DLAs and Lyman-break galaxies (LBGs). If DLAs are gaseous discs surrounding LBGs, and if the apparent brightnesses and impact parameters of the few identified DLAs are representative of the brighter members of the population, then the luminosity distribution of DLAs is nearly flat, and we would expect that some 70 per cent of the galaxy counterparts to DLAs at $z \approx 3$ are fainter than $m_R = 28$.

Key words: galaxies: formation – quasars: absorption lines – quasars: individual: Q0151+048.

1 INTRODUCTION

The quest for non-active galaxies at high redshift has gone through a dramatic change in the last few years. The number of galaxies at $z > 2$ found using the Lyman-break technique (Steidel et al. 1996) is now counted in hundreds, providing information on the global density of star formation at early epochs, and the evolution of galaxy clustering. A different perspective on the formation of galaxies is obtained by studying the population of damped Lyα absorbers (DLAs), the objects responsible for the strongest absorption lines seen in the spectra of quasars. The advantage of DLAs is that they provide a wealth of information on the chemical evolution

of galaxies in the form of the measurement of the metallicity and dust content of the gas (e.g. Lu et al. 1996; Kulkarni & Fall 1997; Pettini et al. 1997). The DLAs have column densities larger than 2×10^{20} cm^{-2}, comparable to the column density for a sightline through the disc of a nearby spiral galaxy. In addition, the total gas content in DLAs is similar to the mass in stars and gas at the present epoch (Wolfe et al. 1995). For these reasons DLAs are widely believed to be the gas reservoirs from which the present spiral galaxies formed.

The relation between DLAs and Lyman-break galaxies (LBGs) is unclear at present, because very few DLAs have been unambiguously detected in emission. At low and intermediate redshifts ($z < 1$) a number of candidate counterparts of DLAs have been discovered in deep images (Steidel et al. 1994, 1995; LeBrun et al. 1997).

*On assignment from the Space Science Department of ESA.

These candidates display a mix of morphological types from spiral galaxies to very compact objects (LeBrun et al. 1997), but so far none has spectroscopic confirmation. At high redshifts there are three DLAs which have been imaged and for which confirmatory spectroscopy exists: the DLA at $z_{abs} = 2.81$ towards PKS 0528–250 (Møller & Warren 1993b), the DLA at $z_{abs} = 3.150$ towards Q2233+131[1] (Djorgovski et al. 1996), and the DLA at $z_{abs} = 4.10$ towards DMS 2247−0209 (Djorgovski, 1998). The first of these has been imaged with the *HST* (Møller & Warren 1998) and has a continuum half-light radius of 0.13 ± 0.06 arcsec, similar to that measured for the LBGs (Giavalisco, Steidel & Macchetto 1996).

Information on the gas sizes of DLAs comes from the measured impact parameters. Combined with the line density of absorbers dn/dz, the space density may be computed. Møller & Warren (1998) produced a preliminary estimate of the space density of high-redshift DLAs by using the impact parameters of confirmed and candidate counterparts. The data suggest that for $q_0 = 0.5$ the space density of DLA clouds at $z > 2$ is more than 5 times the space density of spiral galaxies locally. For $q_0 = 0.0$ there is no evidence as yet that DLA clouds are more common than spiral galaxies locally. A single measurement of 21-cm absorption against an extended radio source, the quasar 0458−020 by Briggs et al. (1989), provides additional information on the size of DLAs. Their analysis indicates that the DLA seen in the spectrum of this quasar has a gas size greater than $8\,h^{-1}$ kpc.

It would clearly be useful to image more high-redshift DLAs, to understand better their relation to LBGs, but also to measure the star formation rates and connect these to the rate of consumption of gas (Pei & Fall 1995). In this paper we present observations of a DLA in the field of the quasar pair Q0151+048A (qA) and Q0151+048B (qB). The two quasars have very similar redshifts, $z_{em} = 1.922$ and 1.937 respectively (Møller, Warren & Fynbo 1998), and an angular separation of 3.27 ± 0.01 arcsec. The spectrum of qA contains a DLA at $z_{abs} = 1.9342$, close to the emission redshift, and so we originally chose this system for study because of the possibility of detecting Lyα emission due to photoionization by either of the quasars (see Møller & Warren 1993a,b for a detailed discussion of the predicted effect). In Møller et al. (1998), we presented a spectrum of qA which shows an emission line in the DLA trough, detected at 4σ. The present paper describes follow-up narrow-band and broad-band imaging observations of this system.

In Section 2 we describe the observations and the data reduction. In Section 3 we describe the PSF-subtraction of qA and qB, and the photometry of the objects found in the field. In Section 4 we discuss the results obtained. Throughout this paper we adopt $q_0 = 0.5$, $H_0 = 100\,h\,\mathrm{km\,s^{-1}\,Mpc^{-1}}$ and $\Lambda = 0$ unless otherwise stated.

2 OBSERVATIONS AND DATA REDUCTION

The data were obtained with the 2.56-m Nordic Optical Telescope (NOT) during four nights beginning 1996 September 15. Observations of the Q0151+048A,B field were done in three bands: the standard *U* and *I* filters, and a special narrow-band filter manufactured by Custom Scientific. The narrow-band filter (CS 3565/20) is tuned to Lyα at the redshift of the DLA, $z = 1.9342$. It has a central wavelength of λ3565 Å and a full-width at half-maximum (FWHM) of 20 Å. The peak transmission of the filter is $T(\lambda)_{max} = 0.385$, and the red leak is less than 10^{-6} to 1.2 μm.

---

[1]When comparing DLA emitters to statistical samples of DLA absorbers, it is important to remember that this object does not meet the N(H I) criterion of a DLA absorber. Statistically speaking, this is a Lyman–limit system.

Table 1. Observations of Q0151+048A,B, 1996 September 15–18.

Filter	Combined seeing	Exposure sec
CS 3565/20	1.1	62700
U	0.9	12000
I	0.8	7800

The CCD used was a 1024^2 backside-illuminated thinned Tektronix with a pixel scale of 0.1757 ± 0.002 arcsec and read noise of $5.4\mathrm{e}^-$. The quantum efficiency in the near UV for this detector rises from 0.3 at 3500 Å to 0.6 at 4000 Å.

Conditions were photometric during most of the run, allowing accurate calibration data to be obtained. The seeing ranged from 0.80 to 1.35 arcsec FWHM in the narrow-band frames, and from 0.60 to 1.30 arcsec FWHM in the *U* and *I* frames. Integration times were in most cases 4000 s for the narrow-band frames, 1000 s for the *U* frames, and 300 s for the *I* frames, ensuring that the noise in each frame is dominated by photon noise from the sky and not by read noise. Between exposures the telescope pointing was jittered in steps of 2 to 5 arcsec to minimize the effect of bad pixels. The total integration times in the different filters are listed in Table 1, together with the measured seeing in the combined frames. For the calibration we observed Landolt (1992) photometric standards for the broad-band data, and the *HST* spectrophotometric standards GD 71, BD+28°4211 and BD+25°4655 (Colina & Bohlin 1994) for the narrow-band data.

Bias and dark frames were first subtracted from the data frames. Twilight sky frames were obtained, and were used to flatten the *U* and *I* data directly. For the narrow-band frames, however, we found that the instrument set-up allowed a small, but significant, amount of light to reach the CCD without passing through the filter. This additional source of background light, which could be either light scattered around the filter wheel or light leaking through the camera enclosure, was too weak to be detectable in the broad-band images, but was a very significant contribution in the narrow-band images. Here we shall refer to this source as scattered light.

The scattered light produced a pattern mostly across the upper two-thirds of the CCD. We applied a correction for this as follows. First the contribution to the twilight sky frames was measured by placing a blocking filter in the filter wheel. From these frames we determined a model of the scattered light by median and Gaussian filtering. This model was then scaled and subtracted from the flat frames prior to the creation of the normalized master-flat. The scattered light in the data frames did not have exactly the same structure across the CCD as in the flat-field frames. The reason for this is not known, but it is possibly due to a different position of the guide probe. We therefore modelled the scattered light in the data frames by summing all the frames, having removed all objects by interpolation and filtering. This model was then scaled to, and subtracted from, the individual data frames. After flat-fielding the residual large-scale variations left were less than 5 per cent.

The frames for each filter were then divided into two groups, depending on whether the seeing was greater or smaller than 1 arcsec FWHM, in order to optimize the combination of the frames. Both groups were then registered by integer pixel shifts to a common coordinate system, and the frames within each group were combined using the optimal combination code described by Møller & Warren (1993b), which maximizes the signal-to-noise ratio (S/N) for faint sources. The model for the scattered light was

Table 2. Measured rms of sky surface brightness. For the narrow band we provide a range due to the presence of the scattered light gradient across the field.

passband	rms SB mag arcsec^{-2}
I(AB)	26.9
u(AB)	25.6
n(AB)	25.7–25.8

included in the calculation of photon noise from the sky. Finally, the two summed frames for each filter were combined by weighting by the inverse of the sky variance.

All magnitudes quoted in this paper are on the *AB* system. The narrow-band data were calibrated directly on to the *AB* system, and magnitudes are denoted *n(AB)*. For the *U* band we determined the colour equation $u = U + 0.26(U - B)$ relating the instrumental magnitude *u* to the standard Johnson *U*. The fit to the *U* colour equation used data for seven different stars, but is not well determined. There was substantial scatter about the fit near $U - B = 0$, ~0.05 mag., and evidence that the relation is non-linear. Such results are typical for this band (e.g. Bessell 1990). The instrumental magnitudes *u* were converted to *AB* magnitudes using the equation $u(AB) = u + 0.49$, determined by integrating the spectrum of the star GD71 over the passband. Here we have retained the lower case *u* for the *AB* magnitude, indicating that the effective wavelength of the filter lies significantly away from the standard value. The colour term for the *I* filter is consistent with zero, i.e., $i = I$, and we used the equation $I(AB) = I + 0.43$ (Fukugita, Shimasaku & Ichikawa 1995) to put the magnitudes on to the *AB* system. Details of the sky noise in the combined images are provided in Table 2.

3 RESULTS

The field of the quasar pair is illustrated in Fig. 1, which shows the final combined *I* (upper) and narrow-band (lower) images. The quasars Q0151+048A,B lie near the centre and are marked qA and qB. Also marked on the image are two bright stars (psfA and psfB) and a source, named S5, to be discussed later (Section 3.4).

3.1 Lyα emission near Q0151 + 048

In the narrow-band image faint emission is seen extending to the east of qA. To get a clearer view of this, in Fig. 2(a) we show a contour plot of a small section from the centre of the narrow-band image. Here, in addition to the images of the two quasars, a plume of emission, presumably Lyα from the DLA, is clearly seen extending towards the east of qA. To reveal the full extent of the Lyα emission, we subtracted the images of the two quasars as follows.

The two bright stars marked psfA and psfB in Fig. 1 were used with DAOPHOT II (Stetson 1994) to define the point spread function (PSF). The complex image made up of the extended Lyα emitter superimposed on the images of the two quasars was decomposed by iteration. First, DAOPHOT II was used to fit, and subtract, the two point sources. Because of the Lyα emission this will oversubtract the point sources. We then used a galaxy model to fit the residuals, finding the minimum-χ^2 fit of the model convolved with the PSF (as in, e.g., Warren et al. 1996). The model consists of an exponential surface-brightness profile $\Sigma = \Sigma_s \exp(-r/r_s)$, and elliptical shape
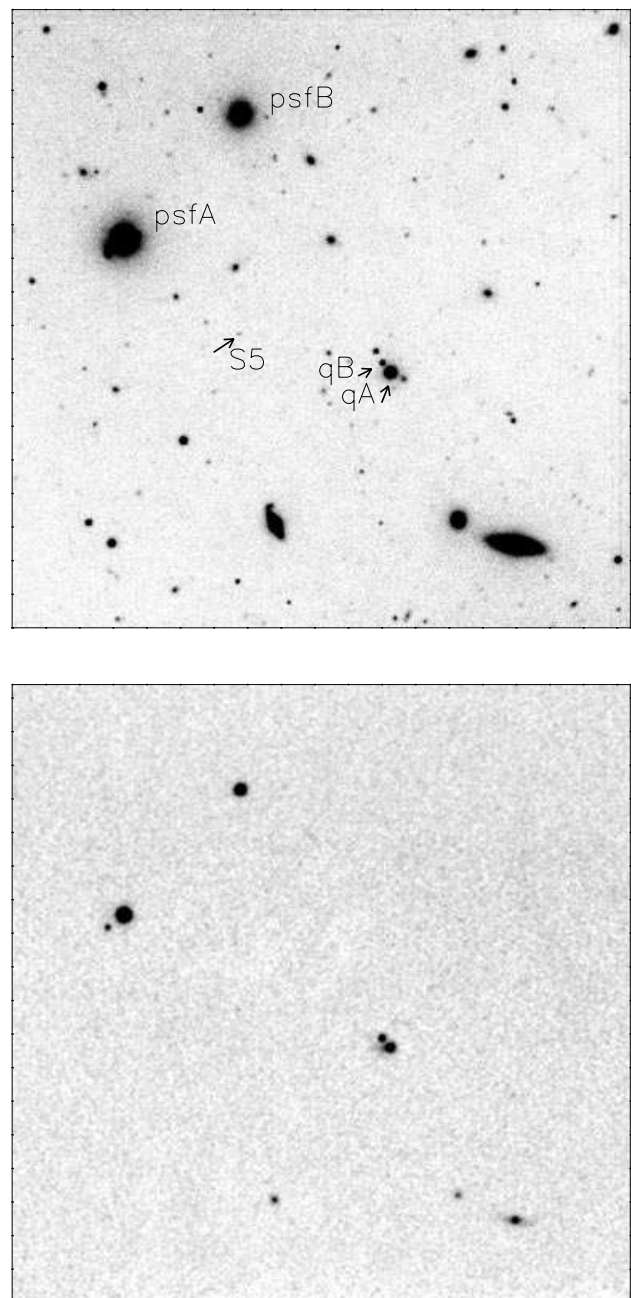

Figure 1. Field containing the quasar pair Q0151+048A,B. *Upper:* combined *I* frame, *Lower:* combined narrow-band frame. The field shown is 920×920 pixels, 162×162 arcsec². North is up, and east to the left. The two quasars are marked qA and qB. The two bright stars marked psfA and psfB were used for determination of the point spread function. The galaxy marked S5 is discussed in the text (Section 3.4).

with constant ellipticity and orientation. Here *r* is equal to $\sqrt{(ab)}$, i.e., the geometric mean of the semimajor and semiminor axes. We tried a range of surface-brightness profiles, but the exponential function provided the best fit. The best-fitting galaxy model was then subtracted from the original image, and a second iteration of DAOPHOT II fitting to the quasar images followed. After nine rounds of alternating point source subtraction and exponential-disc fitting, the procedure reached a stable solution. The frame after subtraction of the images of the two quasars is shown in Fig. 2(b). The parameters of the fit are $r_s = 0.95$ arcsec, a central surface
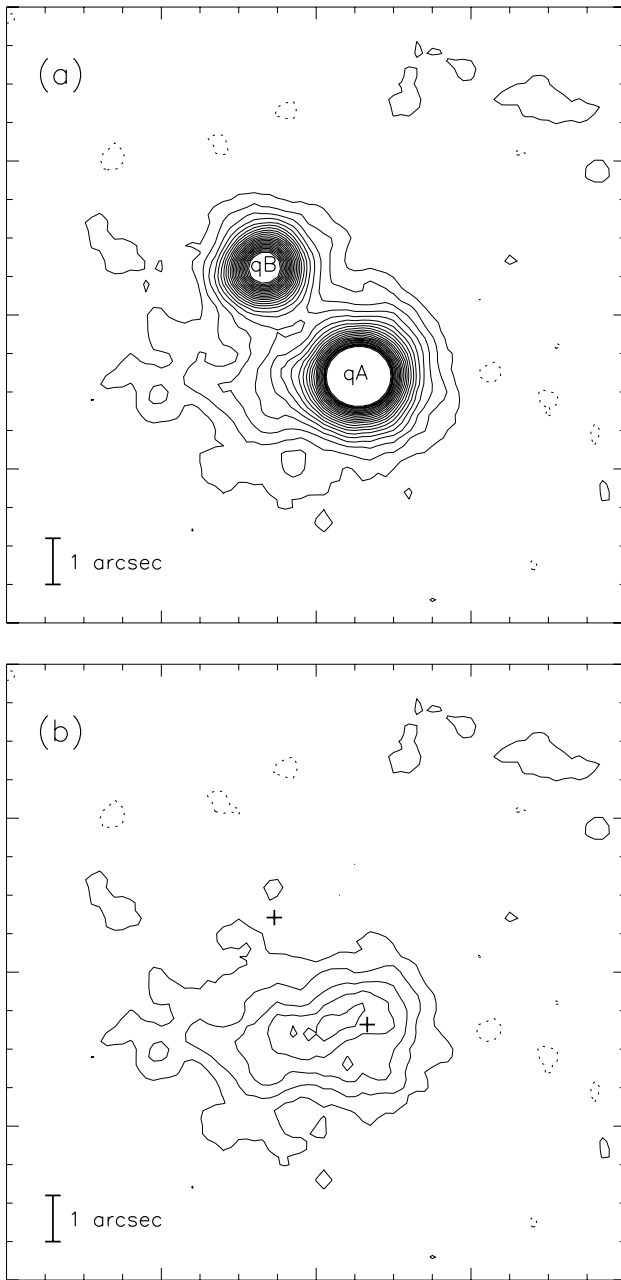
Figure 2. Contour plot of the narrow-band frame showing the 80×80 pixels region, 14×14 arcsec^2, surrounding the two quasars. North is up, and east to the left. The frame has been smoothed by convolution with a Gaussian with σ corresponding to the PSF. (a) Final combined frame showing the two quasars marked qA and qB and excess emission east of qA. The contour levels are at $-3, 3, 6, 9, ... \times 10^{-17}$ erg s^{-1} cm^{-2} arcsec^{-2}, with the dotted contours being negative. (b) Final combined frame (same contour levels as above) after subtraction of the quasar images, revealing Lyα emission from the object S4 over a region 6×3 arcsec^2. The positions where quasar PSFs were subtracted are marked by crosses.

brightness of 3.3×10^{-16} erg s^{-1} cm^{-2} arcsec^{-2}, ellipticity $e = 0.53$, and PA 98° (east of north). The probability associated with the χ^2 of the final fit to the Lyα emission is 4 per cent. This rather small value is explained by the asymmetric light profile, which falls off more sharply to the west than to the east.

In Fig. 2(b) emission is seen from an elongated structure of dimensions approximately 6×3 arcsec^2. In the following we shall

refer to this source of Lyα emission as S4. To perform photometry of objects in the field we used the package SExtractor (Bertin & Arnouts 1996) and determined *isophotal* magnitudes and so called *Automatic Aperture* magnitudes (AAMs), as described below. The magnitudes of the three objects, S4, qA and qB, were measured individually in frames from which the images of the other two objects had been subtracted. The magnitudes of other objects in the vicinity were measured in frames from which all three images had been removed.

With the exception of S4, the apertures for the *isophotal* magnitudes were set by reference to the frame formed by summing the combined frames for the three passbands. This frame was convolved with a Gaussian detection filter with FWHM equal to the seeing. The isophotes set at 1.5 times the noise measured in the unconvolved frame defined the apertures, and the same apertures were then applied to each passband. The detection limit for faint objects was set at a minimum aperture size of 5 pixels (total). Hence the *isophotal* magnitudes provide photometry appropriate for accurate colour determination. For S4 the same procedure was followed, but only the narrow-band frame was used. Finally, since the catalogue is defined by detection in the three-passband combination frame, we also ran SExtractor on the narrow-band frame and found that, with the exception of S4, no source detected in the narrow-band frame at $S/N > 4$ had been overlooked.

The AAM is intended to give the best estimate of the total flux, and is measured using an elliptical aperture with minor axis $b = 2.5r_1\epsilon$ and major axis $a = 2.5r_1/\epsilon$, where r_1 is the first moment of the light distribution, and ϵ is the ellipticity. The isophotal narrow-band magnitude and the AAM for S4 correspond to fluxes of $(9.0 \pm 0.4) \times 10^{-16}$ and $(1.91 \pm 0.07) \times 10^{-15}$ erg s^{-1} cm^{-2} respectively. The AAM for S4 [$n(AB) = 19.95 \pm 0.04$] agrees well with the total magnitude of the fitted galaxy model [$n(AB) = 20.01$].

3.2 Broad-band photometry of S4

Fig. 3(a) shows a contour plot of the *I*-band image of the same field as in Fig. 2. Here we see the two quasars, a star north-east of the quasars which was not visible in the narrow-band image, and two faint galaxies marked gA and gB south-west of the quasar qA. In Fig. 3(b) PSFs have been subtracted at the positions of the two quasars, leaving behind only the star and the two faint galaxies. In Fig. 3(b) we have also overlaid a circle of radius 1.5 arcsec centred on the position of qA. The strong residuals from the PSF-subtraction prevent any detection of additional faint sources within this region.

In Fig. 4(a) we show the *U*-band contour plot of the same region, and in Fig. 4(b) again the field after subtraction of the quasar images. Also, in Fig. 4(b) we have overlaid a circle of radius 1.5 arcsec centred on the position of qA. In the PSFf-subtracted *U* image we see the two faint galaxies gA and gB, but there is also a faint extension about 2 arcsec east of qA, roughly at the position of S4.

The narrow-band image shows that S4 is extended and that it covers the bright quasar qA. Therefore, when observed through a broad-band filter, the tail of the PSF of qA extends across most of S4 and will, even under good seeing conditions, make the determination of broad-band magnitudes of S4 an extremely difficult task. Simple aperture photometry, after fitting and subtracting the quasar PSF, is not possible because of the strong residuals from the PSF-subtraction, and because there is a degeneracy in the determination of how much of the faint extended flux is due to the tail of the quasar psf, and how much is due to S4. In order to break this degeneracy,
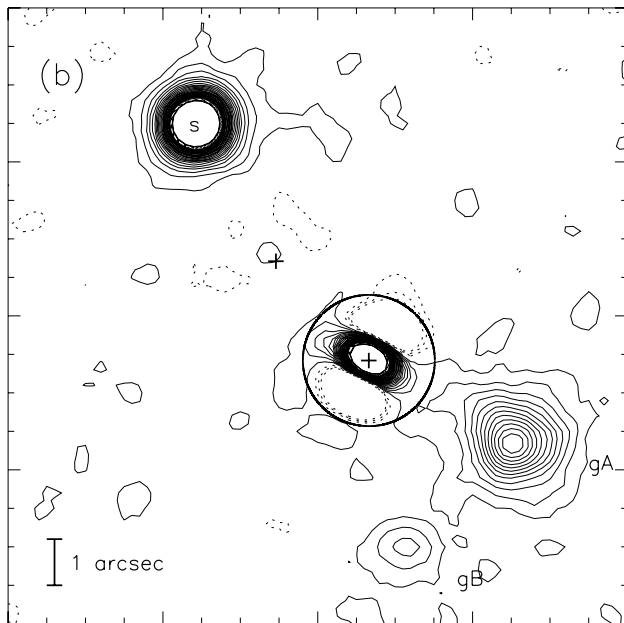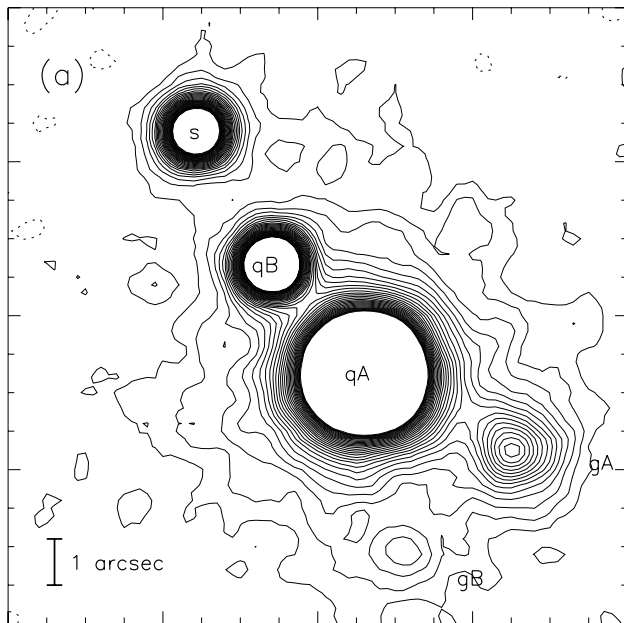
Figure 3. *I*–band contour plot of the same field as in Fig. 2. (a) Final combined frame showing, in addition to the two quasars, two faint galaxies marked gA and gB, and a star marked s. The contour levels are −9, −6, −3, 3, 6, ... × 1σ of the skynoise, with the dotted contours being negative. (b) Final combined frame (same contour levels as above) after subtraction of the quasar images.

Figure 4. *U*-band contour plot of the same field as in Fig. 2. (a) final combined frame showing the two quasars. The contour levels are −9, −6, −3, 3, 6, ... × 1σ of the skynoise, with the dotted contours being negative. (b) Final combined frame (same contour levels as above) after subtraction of the quasar images.

and to obtain an objective measure for the broad-band magnitudes of S4, we proceeded as follows.

On the assumption that the broad-band flux can be fitted by the exponential-disc model defined by the fit to the narrow-band flux, we first subtracted a scaled narrow-band model from the broad-band image. We then subtracted a PSF at the position of qA. The quasar PSF was scaled so that the integrated residual flux measured in a rectangular aperture (5.6 × 3.3 arcsec²), covering both the quasar and the central region of S4, was exactly zero. This calculation was performed for a range of values of the scaling of

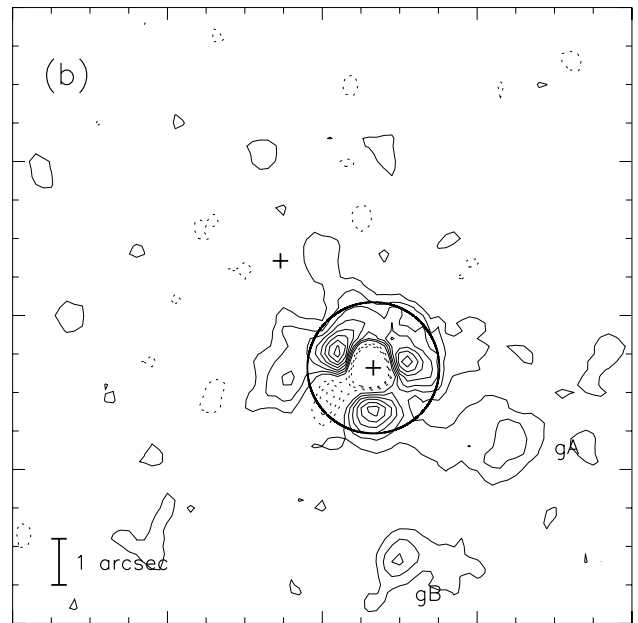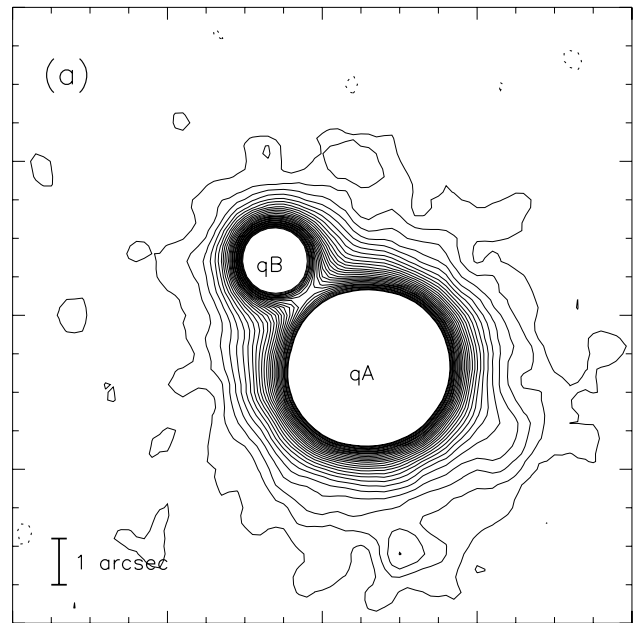the model for S4, and for each combination of S4-model and quasar PSF the total χ^2 of the fit to the data was calculated. The *I* and *U*-band magnitudes of S4 provided in Table 3 are those corresponding to the quasar-PSF/S4-model combinations providing the minimum χ^2. The errors quoted are those where χ^2 increased by one. The rectangular aperture was defined so as not to include flux from the galaxy gA. The χ^2 was calculated in a smaller aperture to exclude the central part of the quasar PSF, where it would be dominated by noise from the strong central PSF-residuals. Table 3 provides a summary of the photometry of the object S4, both quasars, and several other objects found in the field.

Table 3. Photometric properties of the quasars qA and qB, of the faint galaxies S4, S5, gA and gB, and of the star s. Magnitudes of extended objects have been determined in two apertures (isophotal and AAM, both defined in Section 3.1). For the point sources we only provide AAM. Note that magnitudes marked [a] are not true AAM magnitudes, they were determined via scaling of the fitted exponential-disc model as detailed in Section 3.2. Lower limits to magnitudes (upper limits to fluxes) are 2σ. For gA and gB the determination of reliable apertures for AAM was impossible due to the nearness of strong residuals of the QSO PSF-subtraction.

Object	u(AB)	I(AB)	n(AB)	Apert. (pix)
Isoph.				
S4			20.76 ± 0.05	254
S5	24.60 ± 0.10	24.04 ± 0.09	24.1 ± 0.2	37
gA	24.28 ± 0.12	22.00 ± 0.04	> 24.0	170
gB	26.0 ± 0.2	24.88 ± 0.14	> 25.3	18
AAM				
qA	17.90 ± 0.02	17.49 ± 0.02	19.72 ± 0.04	241
qB	21.07 ± 0.03	20.87 ± 0.02	20.04 ± 0.03	241
s	> 25.6	20.98 ± 0.02	> 23.8	341
S4	$22.9^a \pm 0.2$	$22.8^a \pm 0.3$	19.95 ± 0.04	690
S5	24.01 ± 0.09	23.70 ± 0.11	23.6 ± 0.2	241

Møller & Warren (1998) found evidence that a DLA galaxy at $z = 2.81$, as well as its two companion galaxies, all had one (or more) compact cores of continuum emission, while the Lyα emission from the same objects extended over larger areas. If this is a general feature of high-redshift galaxies, we could expect to see one (or several) continuum-emitting cores in S4. Our current data are not adequate to resolve this question; clearly, higher resolution and deeper broad-band imaging is required.

3.3 The impact parameter $b_{\rm DLA}$ of S4

In Møller & Warren (1998) the DLA impact parameter $b_{\rm DLA}$ was defined as the projected distance between the line of sight to the quasar to that of the centroid of the continuum flux of the DLA absorber. In the case of Q0151+048 we clearly see extended Lyα emission from the DLA absorber, and our analysis of the broad-band data shows that they are not inconsistent with a broad band flux distribution identical to that of the Lyα flux. The centroid of the model fit to the narrow-band data is located 0.93 arcsec east, 0.03 arcsec south of Q0151+048A ($b_{\rm DLA,Lyα} = 0.93$ arcsec), and we shall for now adopt this as the impact parameter of the DLA in Q0151+048A.

3.4 Lyα in the surrounding field

An object with Lyα emission at $z = 1.93$ will appear bright in the narrow band compared to U and I, so we can use the results of the photometry to search for other Lyα emitters in the field. In Fig. 5 we plot the n(AB) $- u$(AB) versus n(AB) $- I$(AB) two-colour diagram for all objects detected at a signal-to-noise ratio larger than 4 in the narrow-band frame. Strong Lyα emitters at $z = 1.93$ will lie in the lower left region of this diagram. Conversely, an object with absorption in the narrow-band filter will lie in the upper right corner. Since our narrow-band filter is fairly well centred in the U-band, most objects will have zero n(AB) $- u$(AB) colour, and horizontal lines in Fig. 5 are, to a good approximation, lines of
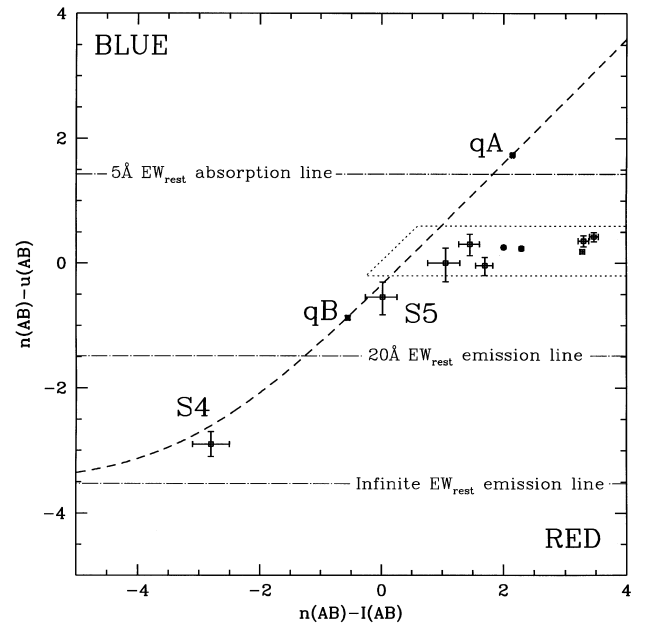

Figure 5. Two-colour diagram n(AB) $- u$(AB) versus n(AB) $- I$(AB) for the 11 detected objects with signal-to-noise ratios in the narrow-band frame > 4. The dashed line is a line of constant $u - I$ in the continuum, indicating that the two quasars have very similar $u - I$ continuum colours but very different Lyα line equivalent widths (EWs). The dotted lines confine the expected region of objects with no special features in the narrow filter. The horizontal lines are lines of constant rest frame EW $= 20$ Å for an emission line at $z = 1.93$ (lower) and rest frame EW $= 5$ Å for an absorption line (upper) that lies in the narrow-band filter.

constant equivalent absorption or emission linewidth. Lines of constant continuum $U - I$ will appear as diagonals in Fig. 5, with the bluest objects in the upper left corner and red objects in the lower right. The dashed curve shows the location of a series of simulated objects with identical power-law continuum on which is superimposed absorption or emission lines of different strengths in the narrow passband. The curve mostly falls along a diagonal of the constant $U - I$ of the continuum, but bends to the left as the emission line starts to dominate the flux in the U-band filter. The dashed curve approaches asymptotically a model with an emission line of infinite equivalent width (dot-dashed line).

The quasar qA lies in the upper part of the diagram, as expected because of absorption by the DLA. Conversely, the quasar qB lies in the lower left part of the diagram. The filter is too narrow to contain all of the Lyα emission line for the quasar qB, but even so the n(AB) $- u$(AB) implies that the mean flux level over the narrow-band filter is at a level 3 times greater than the average over the U band. Therefore the DLA seen in the spectrum of the quasar qA cannot be present in the spectrum of qB. If the quasar qB also lies behind the cloud responsible for the DLA, then the column density is much lower at the position of qB.

There is another candidate Lyα emitter seen in Fig. 5, marked S5. The location of this candidate is shown in Fig 1. The object is detected at S/N ratios of 4.8, 14 and 13 in the narrow-, U- and I-band images respectively. The corresponding flux of the candidate Lyα line is $6.6 \pm 1.3 \times 10^{-17}$ erg cm^{-2} s^{-1} and the rest frame equivalent width of the line is 9 ± 2 Å. The angular separation of S5 from the line of sight to the quasar is 40.9 arcsec, which corresponds to $169\,h^{-1}$ kpc ($q_0 = 0.5$) and $263\,h^{-1}$ kpc ($q_0 = 0.0$) at $z = 1.93$.

Table 4. Measured Lyα luminosities in high-redshift DLAs.

quasar	z_{em}	z_{abs}	luminosity	reference
Q0151+048	1.92	1.93	$1.2 \times 10^{43}\ h^{-2}$	this paper
PKS 0528−250	2.79	2.81	$1.1 \times 10^{42}\ h^{-2}$	Møller & Warren (1993b)
Q2059-360	3.10	3.08	$3.7 \times 10^{42}\ h^{-2}$	Pettini et al. (1995), Leibundgut & Robertson (1999)
Q2233+131	3.30	3.15	$1.2 \times 10^{42}\ h^{-2}$	Djorgovski et al. (1996)

4 DISCUSSION

4.1 The origin of the large Lyα luminosity

The Lyα luminosity of S4 is $1.2 \times 10^{43}\ h^{-2}$ erg s^{-1}. Other high-redshift DLAs for which the Lyα flux has been measured are the DLA at $z = 2.81$ towards PKS 0528−250 (Møller & Warren 1993b), the DLA at $z_{\mathrm{abs}} = 3.150$ towards Q2233+131 (Djorgovski et al. 1996), and the DLA at $z_{\mathrm{abs}} = 3.083$ towards Q2059−360 (Pettini et al. 1995; Robertson & Leibundgut 1998; Leibundgut & Robertson 1999). The last is a spectroscopic detection of spatially resolved excess emission in the DLA absorption trough. The Lyα luminosities for these DLAs are collected in Table 4, and we have assumed a flux of 2×10^{-16} erg s^{-1} cm^{-2} for Q2059−360, based on details in Leibundgut & Robertson (1999). The measured luminosity for Q0151+048 stands out, being several times larger than the other values. In this section we consider possible explanations for this anomaly.

In the light of the dearth of successful detections of emission from DLAs it is noticeable that of the four high-redshift DLAs listed in Table 4, three have redshifts close to the quasar emission redshift. This point was noted by Møller, Warren & Fynbo (1998), who suggested that photoionization by the quasar was a plausible explanation for the Lyα emission for Q0151+048 and Q2059−360, though not for PKS 0528−250 where the continuum emission detected from the DLA is sufficient to account for the Lyα emission (Møller & Warren 1998), and where recent spectroscopic observations (Ge et al. 1997) has ruled out that the quasar could be the source of the ionization. In the case of Q0151+048, there are two quasars potentially close to the DLA galaxy. Q0151+048B is not only close to the line of sight to the DLA galaxy, it also has a redshift (1.937 ± 0.005; Møller et al. 1998) consistent with being identical to that of the DLA galaxy. For this reason, one may slightly favour qB as the source of ionization. Q0151+048A, on the other hand, has a redshift which (if interpreted as due to peculiar motion) indicates that it is moving towards qB and the DLA galaxy with a velocity of about 1200 km s^{-1}. We now consider the possibility of photoionization for the Q0151+048 DLA galaxy in more detail.

The relative distances of qA, qB and the DLA cannot be determined from the redshifts because of peculiar velocities. The DLA lies in front of qA, since it absorbs it, but qB could lie either at larger or smaller distance than the DLA. If qB is beyond the DLA, then the region of high-column density of the absorber does not extend across it. This is because the $n(AB) - u(AB)$ colour of qB corresponds to an average flux level in the n band of 3 times the continuum level (Fig. 5), so the Lyα emission line of qB is not strongly absorbed. One possible explanation for the extended Lyα emission is that qB lies nearer than the DLA and lights up the near face of the absorber (Fynbo, Møller and Warren 1998). However, it is also possible that qA is the source of photoionization. Since qA under this assumption illuminates the backside of the absorber, in the simplest picture one would expect to see a hole in the Lyα emission, containing the line of sight to the quasar, over the area

where the optical depth is high, since over this region the Lyα photons escape out of the back of the absorber. Lyα photons would only be detectable from an annulus around the DLA where the optical depth is approximately unity. However, if DLA clouds are sufficiently inhomogeneous on scales much smaller in extent than the seeing disc, the hole may not be seen as Lyα photons could travel between the densest regions.

The velocity offset of the emission line relative to the DLA for Q0151+048 provides an additional clue to the spatial arrangement of the three objects qA, qB, and S4. The emission line detected for S4 is offset by $\sim$300 km s^{-1} to the blue of the DLA redshift (Møller et al. 1998). In the case of Q2059−360, the emission line lies 490 km s^{-1} to the red of the DLA redshift (Leibundgut & Robertson 1999). One possible explanation of those velocity differences is that they are a consequence of photoionization by the quasar. The radiation pressure of the resonantly scattered Lyα photons would cause the H II skin of the DLA to expand away from the H I in the direction of the quasar (Williams 1972; Urbaniak & Wolfe 1981). This would provide an explanation of why the emission line for Q2059−360 is redshifted relative to the DLA. In this case some of the Lyα photons, produced on the far side, are able to penetrate the cloud because of the reduced optical depth in the red wing of the damped absorption line. Those photons would be observed as a redshifted emission line. For Q0151+048 the blueshift of the emission line would imply that qB is the source of ionizing photons and must lie on the near side of the DLA.

The above arguments are far from conclusive, but the picture that qB is the source of ionizing photons is at least plausible. We can make this statement more quantitative by computing how near qB must lie in order to explain the flux observed. To do this, we follow the analysis presented by Warren & Møller (1996, their equations 1 and 2). Consider a disc of H I of large optical depth, at a distance d from a quasar of absolute magnitude M_B, and with a normal inclined at angle ϕ to the line from the quasar to the cloud. The surface brightness of the cloud over the region of high optical depth is given by

$$\Sigma_{\mathrm{Ly}\alpha} = 3.66 \times 10^{-22} \frac{10^{-0.4 M_B}}{d^2} \frac{\cos\phi}{\alpha} \left(\frac{912}{4400}\right)^{\alpha} \mathrm{erg\ s^{-1}\ cm^{-2}\ arcsec^{-2}},$$

where α is the quasar continuum slope in the power-law representation $f_\nu \propto \nu^{-\alpha}$, and d is in kpc. Therefore the distance of the quasar is given by

$$d = \sqrt{3.66 \times 10^{-22} \frac{10^{-0.4 M_B}}{\Sigma_{Ly\alpha}} \frac{\cos\phi}{\alpha} \left(\frac{912}{4400}\right)^{\alpha}} \ \mathrm{kpc}.$$

We set $\Sigma_{Ly\alpha}$ equal to the peak surface brightness for the model fit to S4 (Section 3) $\Sigma_{Ly\alpha} = 3.3 \times 10^{-16}$ erg s^{-1} cm^{-2} arcsec^{-2}, i.e., where the surface brightness peaks the optical depth of H I visible to the quasar is assumed to be very high, and the drop-off in surface brightness from the peak corresponds to a decline in column density. The absolute magnitude for the quasar is computed from the apparent magnitude $I(AB) = 20.87$ (Table 3). The upper limit to

the distance of qB from the cloud is then obtained by setting $\cos\phi = 1.0$. For values of $\alpha = 0.7$ and 1.0 we find $d < 20$ and $< 14\,h^{-1}$ kpc, respectively, for $q_0 = 0.5$. For $q_0 = 0.0$ the values are $d < 32$ and $< 23\,h^{-1}$ kpc. These values are all the more plausible since they are larger than, but similar to, the projected distance from qB to the DLA, $12\,h^{-1}$ and $19\,h^{-1}$ for $q_0 = 0.5$ and 0.0 respectively. This means that the Lyα emission can be explained by photoionization by qB without having to invoke an unlikely geometry. For example, for $q_0 = 0.5$, setting $\cos\phi = 0.7$, $\alpha = 1.0$, leads to $d = 14.5\,h^{-1}$ kpc, which corresponds to an angle $\theta = 30°$ between the line joining qB to the DLA and the plane of the sky. The boundary of detectable Lyα emission corresponds to the point where the optical depth in H I becomes small. In other words, the quasar is highlighting a Lyman-limit system. The size of the DLA contained would be smaller.

For completeness, we consider the possibility that the photo-ionization model is not correct, and that the Lyα emission is due to star formation. Using the Kennicutt (1983) prescription $SFR = L(H\alpha)/1.12 \times 10^{41}\,\mathrm{erg\,s^{-1}}$ and assuming $L(Ly\alpha)/L(H\alpha) = 10$ and negligible dust extinction leads to

$$SFR = 11(26)\,h^{-2}\mathrm{M_\odot\,yr^{-1}}, \qquad q_0 = 0.5(0.0).$$

However, with this SFR we would expect S4 to have a U-band magnitude of the order $u(AB) = 21$ from the continuum [assuming $SFR = L_{1500}/(1.6 \times 10^{40}\mathrm{erg\,s^{-1}\,\mathring{A}^{-1}})$], which is not seen. Hence, star formation within S4 is very unlikely to be the source of the ionizing photons.

4.2 The relation between DLAs and Lyman-break galaxies

At high redshift, $z \sim 3$, the comoving mass density in neutral gas in the DLAs is similar to the mass density in stars today. In addition, the global star formation rate in the DLAs at high redshift predicted from the rate of decline of the cosmic density of H I (Pei & Fall 1995) is in reasonable agreement with the measured global SFR in the Lyman break galaxies (Madau et al. 1996), given the uncertainties in the two estimates. It is natural therefore to consider the connection between the two populations, DLAs and LBGs. To address this issue, we will make the assumption that every LBG is surrounded by a DLA disc, and ask whether it is then possible to reproduce the measured properties of the high-z DLA population.

A summary of the status of the search for LBGs was given by Dickinson (1999). Fig. 9 in Dickinson (1999) provides the current best estimate of the luminosity function (LF) of galaxies at $z \approx 3$, for $q_0 = 0.5$. This estimate is quite uncertain for two reasons. First it not yet clear how complete the LBG samples are, i.e., how many high-redshift galaxies fall outside their colour-selection criteria. Secondly, the faint-end slope of the LF, i.e., α in the Schechter parametrization, is not well determined, relying as it does on the relatively small number of faint LBGs found in the Hubble Deep Field (HDF). Because of the small field of view of the HDF, and the possibility of normalization errors due to clustering, Dickinson rescaled the HDF numbers to tie smoothly on to the (well-determined) numbers at brighter magnitudes. For the present we will assume that the Schechter fit to the LF present by Dickinson is an adequate representation of the LF of LBGs.

Imagine now that every LBG lies at the centre of a DLA disc. To relate the LBG LF to observables of the DLA population, we will suppose that the size of the DLA disc R_{gas} (i.e., the radius beyond which the column density falls below $2 \times 10^{20}\,\mathrm{cm^{-2}}$) is related to the galaxy luminosity by a power-law relation of Holmberg form

$R_{gas}/R_{gas}^* = (L/L^*)^t$. The value of R_{gas}^* is fixed so as to reproduce the observed line density of DLAs dn/dz, i.e., the average number of DLAs per unit redshift along a line of sight to a quasar. For randomly inclined discs the relation between dn/dz and R_{gas}^* is (Wolfe et al. 1986, equations 7 and 8

$$\frac{dn}{dz} = \frac{\pi}{2}\frac{c}{H}\Gamma(1 + 2t + \alpha)\phi^*(1 + z)^{1/2}R_{gas}^{*2}\,(q_0 = 0.5),$$

where Γ is the gamma function. For randomly inclined discs of radius R the average impact parameter is $\bar{b} = 0.524R$. Therefore

$$\bar{b}^* = 0.524\sqrt{\frac{dn}{dz}\frac{2H}{\pi c\Gamma(1 + 2t + \alpha)\phi^*(1 + z)^{1/2}}} \quad (q_0 = 0.5).$$

At $z = 3$, dn/d$z = 0.27$ (Wolfe et al. 1995). Together with the Holmberg relation, this provides the expected average impact parameter as a function of apparent magnitude, at $z = 3$, and the expected apparent magnitude distribution of a sample of DLAs selected by gas cross-section. Using Dickinson's LF, these results are plotted in Fig. 6, for different values of the parameter t.

When using the predictions presented in Fig. 6, it is important to remember that both the normalization and faint-end extrapolation of the LBG LF are at present poorly known. Also, dn/dz for DLAs could be wrong by a significant factor in cases where systematic effects due to lensing and/or dust obscuration by the DLAs are biasing the number counts. Nevertheless, it is instructive to compare the predicted curves in Fig. 6 to the few detections currently available, and in Fig. 6 we therefore also show the apparent magnitudes and impact parameters of the three confirmed DLA galaxies, and a single DLA galaxy candidate, from which continuum emission has been detected. Apparent magnitudes of the four objects have been transformed to $z = 3$ to enable comparison with the $z = 3$ LBG luminosity function.

We now compare properties of the known DLA galaxies against the predictions, to draw preliminary conclusions about the parameter t. It should be noted first that faint DLAs with small impact parameters would be very difficult to detect, so that the region $m_R > 26$ and $\bar{b} < 4\,h^{-1}$ kpc is so far largely unexplored. On the other hand, DLAs brighter than $m_R = 25$ at impact parameters $\bar{b} > 10\,h^{-1}$ kpc would be detectable from the ground. If $t = 1.0$, most of the LBG counterparts to DLAs would lie in this region, but the few actual detections are fainter and have small impact parameters. Therefore large values of t are not compatible with the observations.

For nearby spirals a value of $t \sim 0.4$ is measured (Wolfe et al. 1986). However, if the measured impact parameters of the few high-redshift DLAs detected are representative of the fraction of DLAs brighter than $m_R = 26$, a lower value of $t \sim 0.25$ is indicated. Referring now to the lower panel of Fig. 6, this would have the consequence that ≈ 70 per cent of the LBG galaxy counterparts to DLAs at $z \approx 3$ are fainter than $m_R = 28$. This conclusion is, in fact, relatively insensitive to the (poorly determined) faint-end slope of the LBG LF. For example, if the actual value is either flatter or steeper than Dickinson's measured value, the curves in the upper panel of Fig. 6 are different, and the value of t that passes through the data points is different. Nevertheless, the corresponding curve in the lower plot for that value of t is quite similar to the lower curve shown.

In the nearby Universe a sample of galaxies selected by gas cross-section has a luminosity distribution peaked near $L*$. The reason why this is probably not the case at high redshifts can be seen as follows. For a Schechter representation of the luminosity function the average luminosity of a sample of galaxies selected by gas
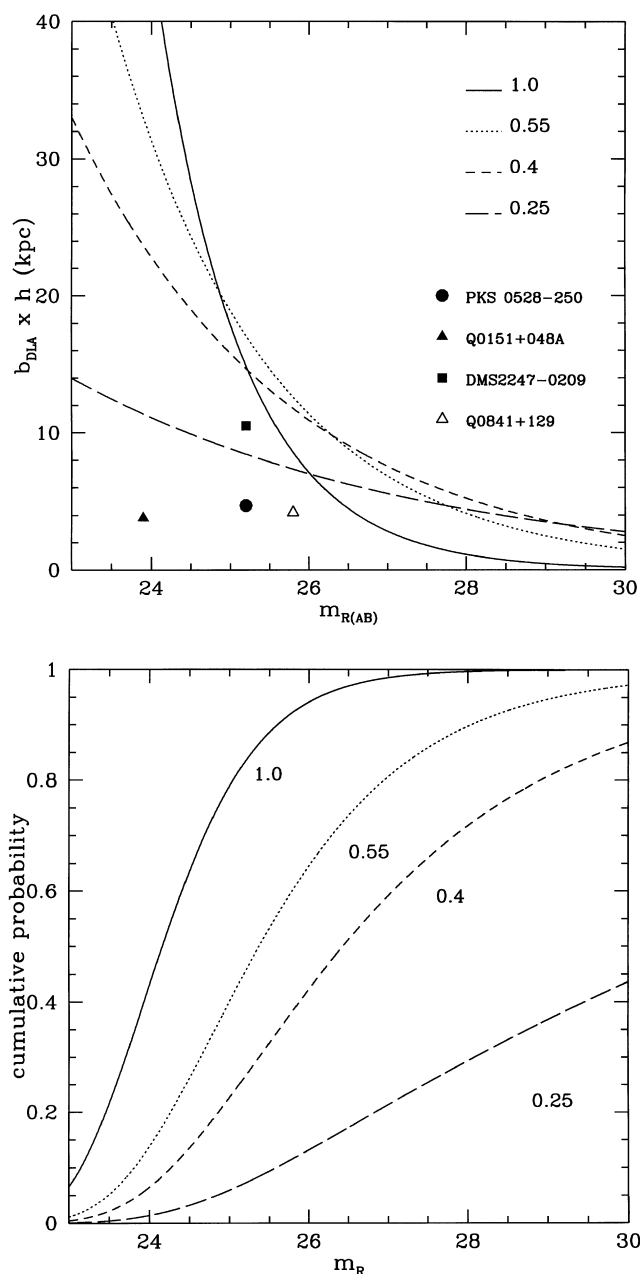
Figure 6. Predicted properties of the DLA population at $z = 3$ if DLAs are gaseous discs surrounding Lyman-break galaxies. *Upper:* the curves show predicted values of the mean impact parameter from the LBG to the line of sight to the quasar for different values of the Holmberg parameter t, as a function of apparent magnitude. The points are measured impact parameters for the three known DLA galaxies (and one likely candidate) for which the continuum magnitude of the galaxy has been measured. *Lower:* the curves show the predicted cumulative probability distribution for the apparent magnitudes of the LBG counterparts to the DLAs.

cross-section is $\bar{L} = L^{*}\Gamma(2 + \alpha + 2t)/\Gamma(1 + \alpha + 2t)$. Locally the canonical numbers for spirals are $\alpha = -1.25$ and $t = 0.4$ (Lanzetta et al. 1991), yielding $\bar{L}(0) = 0.55L^{*}(0)$. At high redshift, taking $\alpha = -1.38$ and $t = 0.25$ gives a much fainter average luminosity $\bar{L}(z) = 0.1L^{*}(z)$. This is a consequence of the fact that at high redshift the faint-end slope of the luminosity distribution $\alpha + 2t$ is closer to the critical value of -1.0, which corresponds to zero average luminosity.

REFERENCES

Bertin E., Arnouts S., 1996, A&AS, 117, 393B
Bessell M. S., 1990, PASP, 102, 1181
Briggs F. H., Wolfe A. M., Liszt H. S., Davis M. M., Turner K. L., 1989, ApJ, 341, 650
Colina L, Bohlin R. C., 1994, AJ, 108, 1931
Dickinson M, 1999, in Livio M., Fall S.M., Madau P., eds, STScI Symp., The Hubble Deep Field, in press
Djorgovski S. G., 1998, in Petitjean P., Charlot S., eds, Structure and Evolution of the IGM from QSO Absorption Lines. Editions Frontières, Paris, p. 303
Djorgovski S. G., Pahre M. A., Bechtold J., Elston R., 1996, Nat, 382, 234
Fukugita M., Shimasaku K., Ichikawa T., 1995, PASP, 107, 945
Fynbo J. U., Møller P., Warren S. J., 1998, in Petitjean P., Charlot S., eds, Structure and Evolution of the IGM from QSO Absorption Lines. Editions Frontières, Paris, p. 408
Ge J., Bechtold J., Walker C., Black J. H., 1997, ApJ 486, 727
Giavalisco M., Steidel C. C., Macchetto F. D., 1996, ApJ, 470, 189
Kennicutt R.C, 1983, ApJ, 272, 54
Kulkarni V. P., Fall S. M., 1997, ApJ, 484, L17
Landolt A. U., 1992, AJ, 104, 340
Lanzetta K. M., Wolfe A. M., Turnshek D. A., Lu L., Mc Mahon R. G., Hazard C., 1991, ApJS, 77, 1
Le Brun V., Bergeron J., Boissé P., Deharveng J. M., 1997, A&A, 321, 733
Leibundgut B., Robertson G., 1999, MNRAS, 303, 711
Lu L., Sargent W. L. W., Barlow T. A., Churchill C. W., Vogt S. S., 1996, ApJS, 107, 475
Madau P., Ferguson H. C., Dickinson M. E., Giavalisco M., Steidel C. C., Fruchter A., 1996, MNRAS, 283, 1388
Møller P., Warren S., 1993a, In Chincarini G., Iovino A., Maccacaro T., Maccagni D., eds, ASP Conf. Ser. Vol. 51, Observational Cosmology. Astron. Soc. Pac., San Francisco p. 598
Møller P., Warren S., 1993b, A&A, 270, 43
Møller P., Warren S., 1998, MNRAS, 299, 661
Møller P., Warren S., Fynbo J., 1998, A&A, 330, 19
Pei Y. C, Fall S. M., 1995, ApJ, 454, 69
Pettini M., Hunstead R. W., King D. L., and Smith L. J., 1995, in Meylan G., ed., QSO Absorption Lines. Springer-Verlag, Berlin p. 55.
Pettini M, King D. L., Smith L. J., Hunstead R. W., 1997, ApJ, 478, 536
Robertson G., Leibundgut B., 1998, in Petitjean P., Charlot S., eds, Structure and Evolution of the IGM from QSO Absorption Lines. Editions Frontières, Paris, p. 271
Steidel C. C., Pettini M., Dickinson M., Persson S. E., 1994, AJ, 108, 2046
Steidel C. C., Bowen D. V., Blades J. C., Dickenson M., 1995, ApJ, 440, L45
Steidel C.C, Giavalisco M., Pettini M, Dickenson M., Adelberger K. L., 1996, ApJ, 462, L17

Stetson P., 1994, User's Manual for DAOPHOT II
Urbaniak J. J., Wolfe A. M., 1981, ApJ, 244, 406
Warren S. J., Hewett P. C., Lewis G. F., Møller P., Iovino A., Shaver P. A., 1996, MNRAS, 278, 139
Warren S., Møller P., 1996, A&A, 311, 25

Williams R. E., 1972, ApJ, 178, 105
Wolfe A. M., Turnshek D. A., Smith H. E., Cohen R. D., 1986, ApJS, 61, 249
Wolfe A. M., Lanzetta K. M., Foltz C. B., Chaffee F. H., 1995, ApJ, 454, 698

This paper has been typeset from a T_EX/L^AT_EX file prepared by the author.